

Physics of the interior of a black hole with an exotic scalar matter

Andrey Doroshkevich,¹ Jakob Hansen,^{2,3} Dmitriy Novikov,^{1,4}
Igor Novikov,^{1,5} Dong-Ho Park,^{2,6} and Alexander Shatskiy¹

¹*Astro Space Center, Lebedev Physical Institute, Russian Academy of Sciences, Moscow, Russia*

²*Korea Institute of Science and Technology Information,
335 Gwahak-ro, Yuseong-gu, Daejeon, 305-806, Korea*

³*Department of Physics, Waseda University, Okubo 3-4-1, Shinjuku, Tokyo, Japan*

⁴*Astrophysics Group, Imperial College, Blackett Laboratory,
Prince Consort Road, London, SW7 2AZ, United Kingdom*

⁵*The Niels Bohr International Academy, The Niels Bohr Institute,
Blegdamsvej 17, DK-2100 Copenhagen, Denmark*

⁶*School of Physics & Astronomy, Seoul National University, Seoul 141-747, Korea*

(Dated: November 27, 2018)

ABSTRACT We use a numerical code to consider the nonlinear processes arising when a Reissner-Nordström black hole is irradiated by an exotic scalar field (modelled as a free massless scalar field with an opposite sign for its energy-momentum tensor). These processes are quite different from the processes arising in the case of the same black hole being irradiated by a pulse of a normal scalar field. In our case, we did not observe the creation of a spacelike strong singularity in the T-region of the space-time. We investigate the antifocusing effects in the gravity field of the exotic scalar field with the negative energy density and the evolution of the mass function. We demonstrate the process of vanishing of the black hole when it is irradiated by a strong pulse of an exotic scalar field.

PACS numbers: 04.70.Bw, 04.25.D-, 95.36.+x

I. INTRODUCTION

The internal structure and physics of black holes (BH) has been the subject of researches during many years [1–37]. A powerful tool for these investigations is to consider a spherical, charged, nonrotating BH which is nonlinearly perturbed by a selfgravitating scalar field. This toy BH model is not very realistic but it shares many properties, including causal structure, with the more realistic rotating BHs.

This toy model has been used in the paper [33] to analyze the physics of the interior of a BH in the case of irradiation by a normal massless scalar field.

The observational apparent acceleration of the universe suggests the presence of a matter field which violates at least the strong and perhaps also the weak energy condition and one of the simplest examples of such energy-conditions-violating matter is a free scalar field with a reversed sign of its energy-momentum tensor, we call this an exotic scalar field. Such an exotic scalar field has previously been used in many works for construction of wormholes in cosmological models with nontrivial topologies, see for example [34, 38, 39]. It would thus be interesting to explore possible implications of such a field to black hole physics.

The goal of this paper is to perform such an analysis, where we will model the exotic matter as described above. We will see that the physics of the interior of a BH which is nonlinearly perturbed by such an exotic scalar field is quite different from the physics of a BH perturbed by normal scalar field.

Rather recently, some aspects of the problem of the internal structure of a BH with unusual scalar fields have been discussed in the papers [40–42], see also references therein.

In the paper [40] the authors discussed the interior structure of a BH arising as a result of the collapse of a spherical charged scalar field shell, taking into account the Hawking radiation. The problem was treated numerically.

In the paper [41] some problems of the inner structure of a BH were discussed using an analytical approach.

Finally, in the paper [42], the authors explored numerically the accretion of a phantom scalar field with a nonzero potential onto a noncharged BH. Especially the variation of the BH area were investigated.

Our approach is different from the above papers. We will address the following points:

- What physical processes arise in the case of irradiation of a charged BH by an exotic scalar field and what is the difference from the case of irradiation by a normal scalar field.
- What kind of singularities arise inside of a charged BH in the case of irradiation by an exotic scalar field.
- How is the the charged BH transformed into an object without horizons in the case of the BH being irradiated by stronger pulses of exotic scalar radiation?
- What are the proper Penrose diagrams for both surviving and nonsurviving (charged) BHs in the case of irradiation by an exotic scalar field.

We will study the nonlinear processes inside the BH using a stable, second order accurate numerical code with

adaptive mesh refinement capabilities. This code was described and tested in details in [34], see also the Appendix A.

This paper is organized as follows:

In section II, Einstein's equations are written for a spherical BH with a fixed magnetic charge and massless scalar fields, both normal and exotic. In section III, we formulate the initial values for our computations. In section IV, we discuss the mass function and some nonlinear processes inside a BH. In section V, we discuss the problem of the origin of strong singularities in a BH. In section VI, we describe our numerical model. In section VII, we remind of the physical processes inside a charged BH irradiated by a pulse of the normal scalar field. In section VIII, we analyze the results of our computations which describe the physics of the interior of a BH with a magnetic field irradiated by a pulse of exotic scalar radiation. In section IX, we discuss the case of irradiation of the BH by both normal and exotic radiation pulses and we summarize our conclusions in section X. Finally, in appendix A, we present results of convergence tests of the numerical code.

II. FIELD EQUATIONS FOR THE SPHERICAL MODEL

We wish to investigate the evolution of a spherical BH with a fixed magnetic or electric charge q (i.e. Reissner-Nordström metric) under the action of pulses of selfgravitating, massless scalar fields, both normal Φ (with a positive energy density, $\varepsilon > 0$) and exotic Ψ (with a negative energy density, $\varepsilon < 0$). The general equations for the analysis were written in [34].

The line element in double-null coordinates can be written as

$$ds^2 = -2e^{2\sigma(u,v)} du dv + r^2(u,v) d\Omega^2, \quad (1)$$

where $\sigma(u,v)$ and $r(u,v)$ are functions of the null coordinates u and v (in- and out-going respectively). The nonzero components of the Einstein-tensor are:

$$G_{uu} = \frac{4r_{,u}\sigma_{,u} - 2r_{,uu}}{r} \quad (2a)$$

$$G_{vv} = \frac{4r_{,v}\sigma_{,v} - 2r_{,vv}}{r} \quad (2b)$$

$$G_{uv} = \frac{e^{2\sigma} + 2r_{,u}r_{,v} + 2rr_{,uv}}{r^2} \quad (2c)$$

$$G_{\theta\theta} = -2e^{-2\sigma}r(r_{,uv} + r\sigma_{,uv}) \quad (2d)$$

$$G_{\varphi\varphi} = -2e^{-2\sigma}r \sin^2\theta(r_{,uv} + r\sigma_{,uv}) \quad (2e)$$

The energy-momentum tensor can be written as a sum of contributions from the exotic scalar field Ψ (with the negative energy density), from the normal scalar field Φ (with the positive energy density) and from the ordinary

electro-magnetic field, i.e. : $T_{\mu\nu} = T_{\mu\nu}^{\Psi} + T_{\mu\nu}^{\Phi} + T_{\mu\nu}^{em}$:

$$T_{\mu\nu}^{\Psi} = \frac{-1}{4\pi} \begin{pmatrix} \Psi_{,u}^2 & 0 & 0 & 0 \\ 0 & \Psi_{,v}^2 & 0 & 0 \\ 0 & 0 & r^2 e^{-2\sigma} \Psi_{,u} \Psi_{,v} & 0 \\ 0 & 0 & 0 & r^2 \sin^2\theta e^{-2\sigma} \Psi_{,u} \Psi_{,v} \end{pmatrix} \quad (3)$$

$$T_{\mu\nu}^{\Phi} = \frac{+1}{4\pi} \begin{pmatrix} \Phi_{,u}^2 & 0 & 0 & 0 \\ 0 & \Phi_{,v}^2 & 0 & 0 \\ 0 & 0 & r^2 e^{-2\sigma} \Phi_{,u} \Phi_{,v} & 0 \\ 0 & 0 & 0 & r^2 \sin^2\theta e^{-2\sigma} \Phi_{,u} \Phi_{,v} \end{pmatrix} \quad (4)$$

$$T_{\mu\nu}^{em} = \frac{q^2}{8\pi r^4} \begin{pmatrix} 0 & e^{2\sigma} & 0 & 0 \\ e^{2\sigma} & 0 & 0 & 0 \\ 0 & 0 & r^2 & 0 \\ 0 & 0 & 0 & r^2 \sin^2\theta \end{pmatrix} \quad (5)$$

The $u-u$, $v-v$, $u-v$ and $\theta-\theta$ components of the Einstein equations (with $c=1$, $G=1$) respectively are:

$$r_{,uu} - 2r_{,u}\sigma_{,u} - r(\Psi_{,u})^2 + r(\Phi_{,u})^2 = 0 \quad (6)$$

$$r_{,vv} - 2r_{,v}\sigma_{,v} - r(\Psi_{,v})^2 + r(\Phi_{,v})^2 = 0 \quad (7)$$

$$r_{,uv} + \frac{r_{,u}r_{,v}}{r} + \frac{e^{2\sigma}}{2r} \cdot \left(1 - \frac{q^2}{r^2}\right) = 0 \quad (8)$$

$$\sigma_{,uv} - \frac{r_{,v}r_{,u}}{r^2} - \frac{e^{2\sigma}}{2r^2} \cdot \left(1 - \frac{2q^2}{r^2}\right) - \Psi_{,u}\Psi_{,v} + \Phi_{,u}\Phi_{,v} = 0 \quad (9)$$

The scalar fields satisfy the Gordon-Klein equation $\nabla^{\mu}\nabla_{\mu}\Psi = 0$ and $\nabla^{\mu}\nabla_{\mu}\Phi = 0$, which in the metric (1) become:

$$\Psi_{,uv} + \frac{1}{r}(r_{,v}\Psi_{,u} + r_{,u}\Psi_{,v}) = 0 \quad (10)$$

$$\Phi_{,uv} + \frac{1}{r}(r_{,v}\Phi_{,u} + r_{,u}\Phi_{,v}) = 0 \quad (11)$$

Equations (8)-(11) are evolution equations which are supplemented by the two constraint equations (6) and (7). It is noted that none of these equations depend directly on the scalar fields Ψ and Φ but only on their derivatives, i.e. the derivative of the scalar field is a physical quantity, while the absolute value of the scalar field itself is not. Specifically we note the $T_{uu}^{\Psi} = -(\Psi_{,u})^2/(4\pi)$ and $T_{vv}^{\Psi} = -(\Psi_{,v})^2/(4\pi)$ components of the energy-momentum tensor (3) and $T_{uu}^{\Phi} = (\Phi_{,u})^2/(4\pi)$ and $T_{vv}^{\Phi} = (\Phi_{,v})^2/(4\pi)$ components of the energy-momentum tensor (4), which are part of the constraint equations. Physically T_{uu} and T_{vv} represents the flux of the scalar field through a surface of constant v and u respectively.

III. INITIAL-VALUE PROBLEM

We wish to evolve the unknown functions $r(u,v)$, $\sigma(u,v)$, $\Phi(u,v)$ and $\Psi(u,v)$ throughout some computational domain. We do this by following the approach

of [18, 20, 23, 24, 27, 29, 33, 34, 43, 44] to numerically integrate the four evolution equations (8)-(11) along the characteristics. These equations form a well-posed initial-value problem and in the double-null coordinate we use, it is most natural to use the characteristic initial-value formulation in which the initial values of the unknown functions are specified on two initial null segments, namely an ingoing ($v = v_0 = \text{constant}$) and an outgoing ($u = u_0 = \text{constant}$) segment [43].

Our code is a free evolution code, i.e. we impose the constraint equations (6) and (7) only on the initial segments, consistency of the evolving fields with the constraint equations is then ensured via the contracted Bianchi identities [43]. However we use the constraint equations throughout the domain of integration to check the accuracy of the numerical simulation.

We are free to choose the distribution of the Φ and Ψ -fields on the initial null segments, our choices are described in section VI. We are also free to choose $r(u, v)$ on the initial surfaces, this merely expresses the gauge freedom associated with the transformation $u \rightarrow \tilde{u}(u), v \rightarrow \tilde{v}(v)$ (the line element (1) and the equations (6)-(11) are invariant to such a transformation). Hence, the only variable left for us to determine on the initial surfaces is σ . This can easily be found by integrating the constraint equations eq. (6) and (7), which ensures that the constraint equations are satisfied on the initial hypersurfaces. Specifically on the outgoing $u = u_0$ hypersurface it is found by the integral:

$$\sigma(u_0, v) = \sigma(u_0, v_0) + \int_{v_0}^v \frac{r_{,vv} - r (\Psi_{,v})^2 + r (\Phi_{,v})^2}{2r_{,v}} dv \quad (12)$$

where $\sigma(u_0, v_0)$ is an integration constant. We follow [27, 29, 33, 34, 43] and set $\sigma(u_0, v_0) = \ln\left(\frac{1}{\sqrt{2}}\right)$ throughout the paper. The initial data along the ingoing surface, is set in a similar manner.

Hence, by specifying a distribution of the scalar fields Φ and Ψ on the initial null segments, choosing a gauge, integration constant $\sigma(u_0, v_0)$, charge and mass parameters "q" and "m" (these relate to the gauge, see eq. (13) and section VI) we can specify complete initial conditions on the initial null segments. Using the numerical code from [34], we can then use the evolution equations, eqs. (8)-(11), to evolve the unknown functions along the characteristics, throughout the computational domain. Our specific choices for initial conditions are described in sec. VI.

Finally, we wish to emphasize that a consequence of evolving along the characteristics in our double-null coordinate, spherical model, is that the specification of initial data along in- and outgoing null surfaces fully defines the initial-value problem. Thus, there is no need to specify any additional boundary conditions, the initial values along the null surfaces *are* the boundary conditions. For further details on the numerical code, see [34] and references therein.

IV. MASS FUNCTION

The evolution of the interior of a BH with a scalar field is highly nonlinear. An important characteristic of this evolution is the mass function. This function represents the total mass (without the magnetic field) in a sphere of radius $r(u, v)$ (see [10, 20, 24, 43]). In the metric (1), the mass function is (see [27, 30]):

$$m = \frac{r}{2} \left(1 + \frac{q^2}{r^2} + \frac{2r_{,u}r_{,v}}{e^{2\sigma}} \right) \quad (13)$$

In the metric

$$ds^2 = g_{tt} dt^2 + g_{rr} dr^2 + r^2 d\Omega^2 \quad (14)$$

the mass function m has the form

$$m = \frac{r}{2} \left(1 + \frac{q^2}{r^2} - g_{rr}^{-1} \right) \quad (15)$$

There are two physical processes which can lead to a nonlinear change of the mass function:

1. The mass m inside a sphere can change because of the work of the pressure forces acting on the surface of the sphere.

2. Mass inflation can occur [10].

Both processes have been described in [33]. We want to emphasize that in the case of the exotic scalar field we should take into account the negative energy density and negative radial pressure of the exotic scalar field. Of course, in addition to the above mentioned processes, there is also the trivial process of matter flowing into the sphere. We will discuss the properties of the mass function in our model in the subsequent sections.

One more important nonlinear process is the focusing effect caused by the gravity of pulses of opposite fluxes of radiation (see [33]). In our case of radiation pulses with negative energy densities, it is rather a defocussing effect. Its manifestation will be discussed below.

V. STRONG SINGULARITY

In the case of nonlinear perturbations of the initial BH by the normal Φ scalar field, a strong spacelike singularity arises in a T-region as a result of the nonlinear processes (see for example [13, 33, 45]).

We want to remind of the classification of R - and T -regions in space-times with spherical symmetry [46–48]. The R -regions are regions where world-lines $r = \text{const}$ are timelike. The T_+ -regions are regions where world-lines of $r = \text{const}$ are spacelike and the direction to larger r is in the direction to the future. The T_- -regions are regions where world-lines of $r = \text{const}$ are spacelike and the direction to smaller r is in the direction to the future. The R - and T -regions are separated by apparent horizons which are defined by locations where $\frac{dr}{dv} = 0$ or $\frac{dr}{du} = 0$.

The strong singularity under discussion exists together with a weak null singularity (instead of the inner horizon of a Reissner-Nordström BH [12]).

In the case of nonlinear perturbations of the initial BH by the exotic Ψ -field the situation is quite different.

First of all, the analysis in [49] have demonstrated that in the case of a Ψ field in the vicinity of the singularity $r = 0$, we can neglect the influence of the exotic scalar field Ψ comparative to the influence of the magnetic field. This means that the singularity $r = 0$ is of a Reissner-Nordström type. It is a timelike singularity and it is in an R-region. A spacelike strong singularity $r = 0$ in a T_- -region is not possible.

Secondly, we will see in the subsequent sections that under the action of the irradiation by the exotic scalar field, the T_- -region becomes smaller and smaller when the intensity of the irradiation increases, even in the case when the BH still survives. We can see practically all of the T_- -region in our computational domain and definitely there are not any strong singularities in the T_- -region. On the other hand, a strong timelike singularity of the Reissner-Nordström type must exist in the R-region outside of our computational domain.

We will consider the problems of the singularities in some detail in the following sections.

Finally, we wish to note that no special treatment is needed in order for our numerical code to successfully handle the spacelike $r = 0$ singularities that occur in our computations. The characteristic evolution of our numerical code means that only points which are causally connected to a singularity can “see” the singularity, but since no points are causally connected to a spacelike $r = 0$ singularity, they pose no problem. Timelike and coordinate ($r = 0$) singularities, on the other hand, *do* pose a problem in principle as these points are causally connected to the rest of the space-time. In practice, however, it is not a problem since we choose our initial conditions in such a way that they do not include the coordinate singularity (cf. sec. VI) and any timelike singularity are outside of our computational domain.

For further details on the workings of our numerical code, please see [34] and references therein.

VI. THE MODEL

In the subsequent sections we investigate the fully nonlinear processes in the spherical charged BH irradiated by a pulse of the exotic scalar field Ψ (and in section IX irradiated by both Ψ and Φ pulses). For that we use the results of our numerical simulations. Our numerical code is thoroughly described and tested in [34], here we just mention that the code uses Adaptive Mesh Refinement (AMR) in both u - and v -coordinates and is second order accurate. About the convergence of the code in the case of the present model, see Appendix A.

Our choice of the initial values corresponds to the following physical situation; There is a BH with a magnetic field and at some distance from the horizon, at the initial moment, there is a rather narrow spherical layer of an in-falling scalar field.

Throughout this paper, prior to the irradiation by the scalar pulses, the BH has initial mass $m_0 = 1$ and charge $q = 0.95m_0$. For the simulations, the domain of integration as a rule is $5 \leq v \leq 30$, $0 \leq u \leq 30$ and we choose a standard gauge in which r is linear in v and u on the initial null segments. Specifically, our gauge choice is:

$$r(u_0, v) = v \quad r(u, v_0) = r(u_0, v_0) + r_{,u} u \quad (16)$$

where $r_{,u}$ is determined from the mass function, eq. (13), at the initial moment u_0, v_0 , to ensure consistency. We note that this computational domain does not include the $r = 0$ coordinate singularity.

For our numerical experiments we specify various initial conditions. Along the ingoing border $v_0 = 5$, the initial values for all simulations correspond to the (Reissner-Nordström) BH solution with $m_0 = 1$ and $q = 0.95m_0$ without any additional fields. Along the outgoing border $u_0 = 0$, we vary the initial conditions in such a way as to imitate some physical fluxes of the fields Φ and Ψ into the charged BH.

We specify the pulses of the scalar fields in the form:

$$\Phi_{,v}(u_0, v) = A_\Phi \sin^2 \left(\pi \frac{v - v_{\Phi 0}}{v_{\Phi 1} - v_{\Phi 0}} \right), \quad (17)$$

$$\Psi_{,v}(u_0, v) = A_\Psi \sin^2 \left(\pi \frac{v - v_{\Psi 0}}{v_{\Psi 1} - v_{\Psi 0}} \right), \quad (18)$$

where A_Φ and A_Ψ , $v_{\Phi 0}$, $v_{\Phi 1}$, $v_{\Psi 0}$, $v_{\Psi 1}$ are constants. Outside the interval $(v_{\Phi 0}, v_{\Phi 1})$ we have $\Phi_{,v}(u_0, v) = 0$. Outside the interval $(v_{\Psi 0}, v_{\Psi 1})$ we have $\Psi_{,v}(u_0, v) = 0$.

If the fluxes through the two initial surfaces u_0 and v_0 have been chosen, as was described in section III, all other initial conditions are determined by our choice of gauge and the constraint equations.

VII. PHYSICAL PROCESSES INSIDE OF THE CHARGED BLACK HOLE IRRADIATED BY A PULSE OF NORMAL RADIATION

We start from reminding of what happens if we irradiate a charged BH with a pulse of the normal scalar field with a positive energy density [18, 19, 27, 29, 33].

We described the corresponding processes in detail in [33], here we summarize main effects:

1) When the positive energy pulse crosses the outer apparent horizon (OAH), the horizon becomes bigger. When the pulse crosses the inner apparent horizon (IAH1), it becomes smaller.

After the passage of the pulse, the mass function increases by an amount corresponding to the energy contained within the pulse. These effects are the trivial consequences of mass being pumped into the BH by the initial pulse.

2) Next is the focusing effect. Any test photons propagating along the null-geodesic lines $u = const$ and $v = const$ are under action of the gravity of the fluxes T_{vv}

and T_{uu} respectively. The last arises as a result of the scattering of the ingoing T_{vv} radiation by the space-time curvature. In the subsequent evolution these T_{vv} and T_{uu} fluxes are converted into one another due to the curvature of the space-time. The gravity of T_{vv} and T_{uu} leads to a focusing effect on the test photons. In the absence of the scalar radiation, outgoing photons along $u = \text{const}$ slightly inside IAH1 will go to greater r as v increases in the Reissner-Nordström solution. With the existence of the scalar radiation, a similar outgoing ray will now, because of the focusing effect, go to smaller r and generate a maximum $\left. \frac{du}{dv} \right|_{r=\text{const}} = 0$ in the $u - v$ coordinates. This corresponds to the position of the apparent horizon. As a result the position of IAH1 changes dramatically. It goes up sharply with increasing v coordinate.

3) Now we consider the properties of the mass function. For late (big) u the mass function along the lines $u = \text{const}$ demonstrates a sharp increase with growing v . This is the result of the compression which tends to infinity. As a consequence, a strong singularity $r = 0$ arises and these lines, $u = \text{const}$, come to the singularity $r = 0$. The Kretschmann scalar ($K = R_{\alpha\beta\gamma\delta}R^{\alpha\beta\gamma\delta}$), which is the curvature characteristic of the space-time, also increases sharply along these lines, due to the infinite compression.

For smaller u the lines $u = \text{const}$ go to the Cauchy horizon IAH1 at $v \rightarrow \infty$. The increase of the mass function along these lines is mainly due to the mass inflation and is exponential when $v \rightarrow \infty$. The mass inflation is the basic process in the formation of the weak singularity instead of the inner smooth Cauchy horizon.

The weak null singularity shrinks down due to the focusing effect from the gravity of the T_{uu} radiation and finally comes down to $r = 0$.

VIII. PHYSICAL PROCESSES INSIDE OF A CHARGED BLACK HOLE IRRADIATED BY A PULSE OF EXOTIC SCALAR RADIATION

Now let us compare the processes described in the previous section with the processes in the case when a Reissner-Nordström BH is irradiated by an exotic scalar field.

A. The case of survival of the BH

We start from the case when the power of the exotic radiation pulse is rather weak and the BH survives after being irradiated. Let us first consider the following case:

$$A_\Phi = 0,; \quad A_\Psi = 0.01 \quad (v_{\Psi 0} = 5, \quad v_{\Psi 1} = 9). \quad (19)$$

We will see that total amount of negative mass pumped into the BH in this case is rather small, it survives but the positions of the apparent horizons change.

It is clearly seen from fig. 1(a) and fig. 1(b) that the result of the processes with the negative energy density pulse is opposite to the case of a positive energy density

pulse described above. When the pulse of the negative energy density crosses the OAH, the horizon becomes smaller and on the corresponding plot (Fig. 1(a)) it can be seen to be going to higher u (corresponding to smaller r , cf. eq. (16)) in the region $5 < v < 9$.

Before the pulse at $v < 5$, the mass of the BH was $m = 1$ and the position of the OAH corresponded to $u = 23.190$. After the end of the process, the final position of the OAH corresponds to $u \approx 23.206$ (fig. 1(a)) and the final asymptotic external mass is $m \approx 0.998$ (as we will see in fig. 2(a)).

We formulated the initial conditions along the outgoing null surface $u = 0$. When the ingoing radiation pulse propagates from $u = 0$ to the OAH, it experiences scattering because of the curvature of the space-time, thus being converted into outgoing radiation. At later times, that scattered radiation is then rescattered and being converted back into ingoing radiation and so on and so forth. The tail of this scattered radiation thus reaches the OAH at later times. This can be observed in fig. 1(a)) where the OAH can be seen to change its position in two steps.

We would like to emphasize that the scattering and the rescattering are the result of interaction of the propagating field with the curvature of the space-time background but not any boundary conditions.

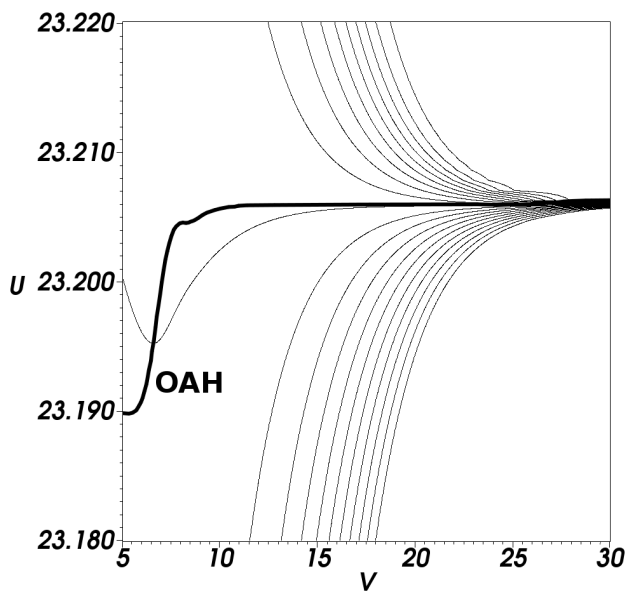
The first step, when the initial pulse passes into the BH, can be observed between $5 \lesssim v \lesssim 9$, and the second step (caused by the scattered radiation) can be observed between $9 \lesssim v \lesssim 11$.

When the pulse crosses the IAH1, the effects are again opposite to those of an energy pulse with a positive energy density and the horizon thus becomes bigger (goes to smaller u) in the region $5 < v < 9$ (Fig. 1(b)).

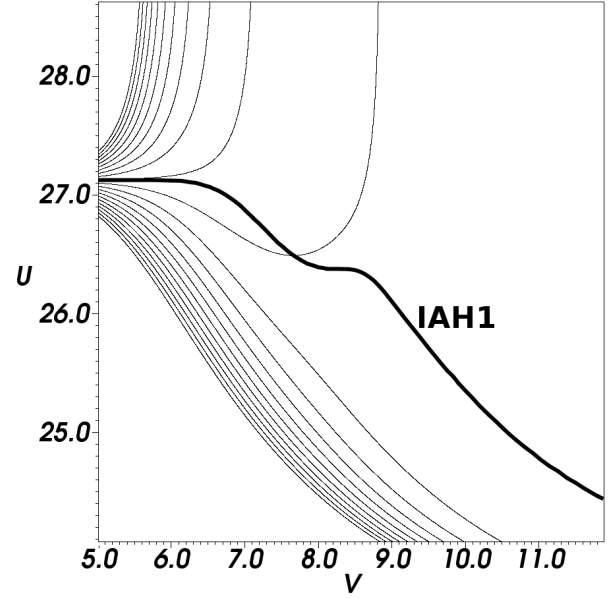
In the region $v \gtrsim 9$ in Fig. 1(b), the internal horizon IAH1 is seen to go to smaller u (higher r). This is the manifestation of the antifocusing gravitational effects which are opposite to the effect 2), mentioned above in the discussion of the positive energy density pulse (see section VII).

The behavior of the mass function inside the pulse in the region $5 \lesssim v \lesssim 9$, (shown in Fig. 2(a) along lines of constant u), is also opposite to the case of an ingoing pulse with positive energy density described in section VII, in that the mass function decreases as the pulse enters the BH. This is also the case for pulses with higher (negative) energy contents (Fig. 2(b)). In Fig. 2(a) it can be seen that the mass function along the line $u = 0$ (where we formulate the initial conditions) is lower than along the line $u = 23$ (slightly outside of the OAH). This is the manifestation of the scattering processes outside the BH. Because of the scattering process, only part of the energy along $u = 0$ will actually reach the OAH near $u = 23$, the rest will be converted into outgoing radiation that will forever escape from the BH.

The consequence of the concentration of the incoming energy near the inner Cauchy horizon, is still the same as it was in the case of the positive energy density pulse. This concentration can be seen in Fig. 3(a) where lines

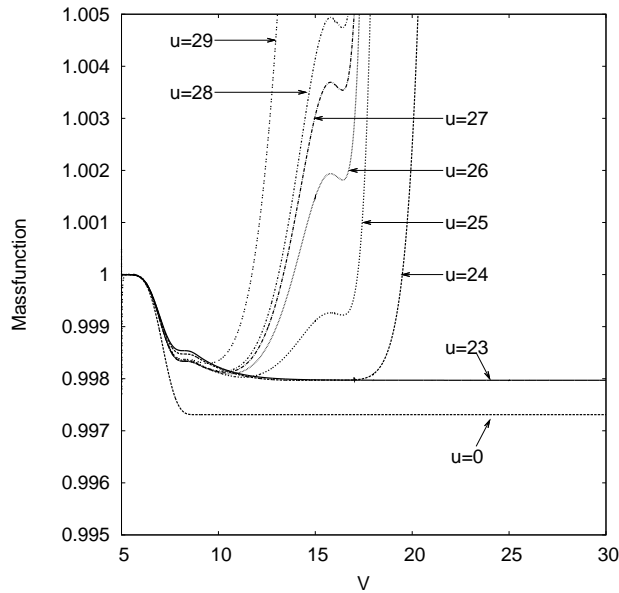


1(a): Thick line is position of OAH. Thin lines are lines of constant r (values decreasing from bottom to top).

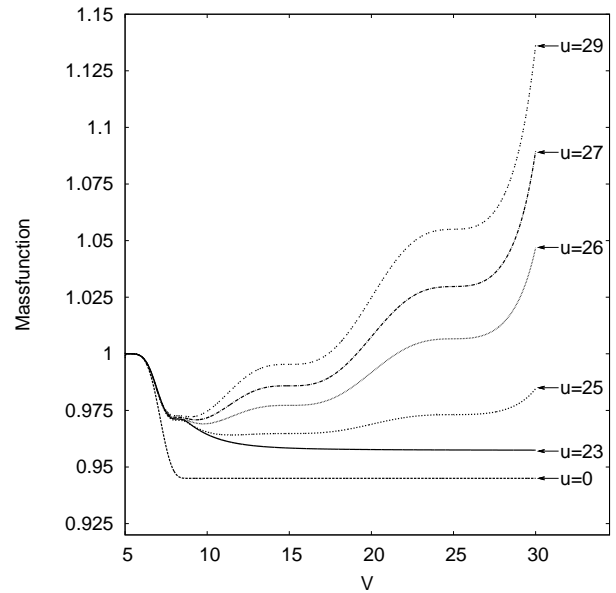


1(b): Thick line is position of IAH1. Thin lines are lines of constant r (values decreasing from bottom to top).

FIG. 1: Positions of the apparent horizons for the case : $A_\Phi = 0$; $A_\Psi = 0.01$, ($v_{\Psi_0} = 5$, $v_{\Psi_1} = 9$). When pulse of the negative energy crosses the outer apparent horizon (OAH), it becomes smaller and the inner apparent horizon (IAH1) becomes larger.

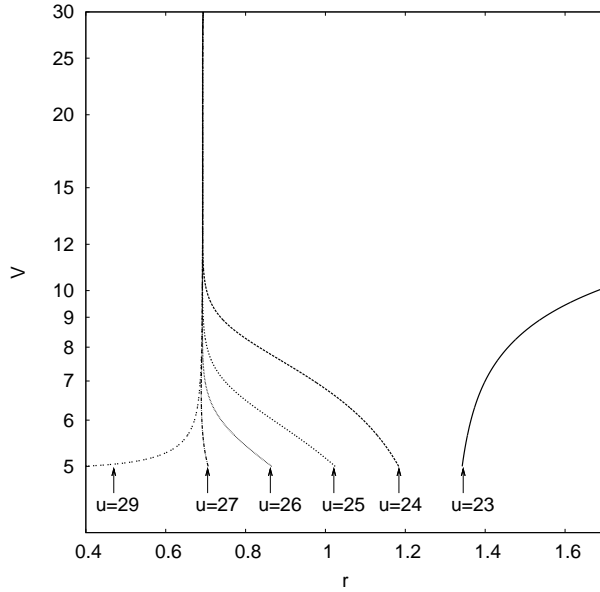
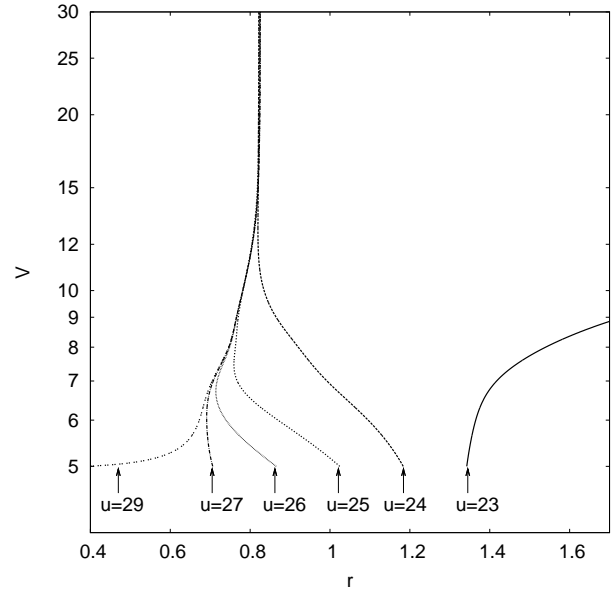
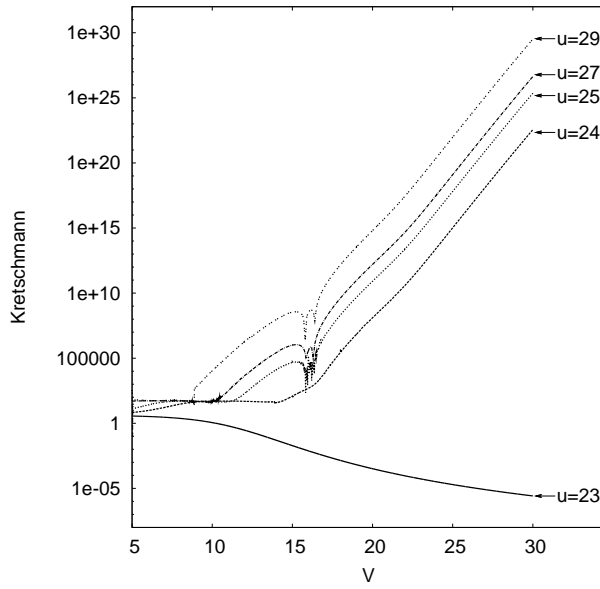
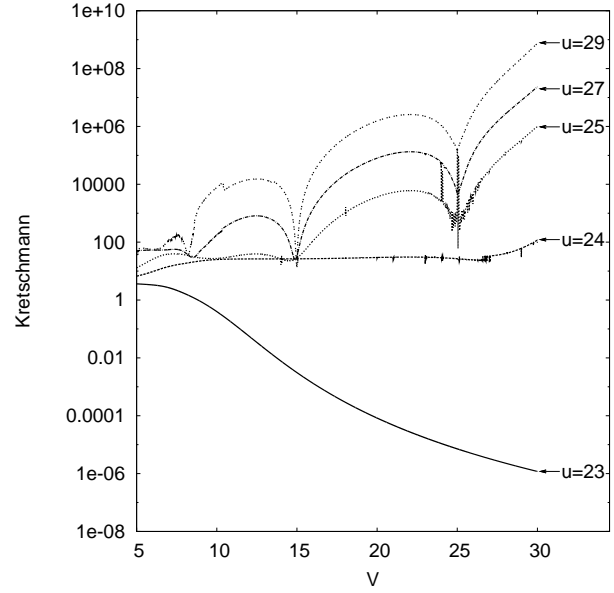


2(a): Case: $A_\Phi = 0$; $A_\Psi = 0.01$, ($v_{\Psi_0} = 5$, $v_{\Psi_1} = 9$).



2(b): Case: $A_\Phi = 0$; $A_\Psi = 0.045$, ($v_{\Psi_0} = 5$, $v_{\Psi_1} = 9$).

FIG. 2: The mass function along lines of constant u for two cases of weak pulses. One can see the decrease of the mass function caused by the pulse of negative energy and the increase of it that results from the mass inflation.

3(a): Case: $A_\Phi = 0$; $A_\Psi = 0.01$, ($v_{\Psi 0} = 5$, $v_{\Psi 1} = 9$).3(b): Case: $A_\Phi = 0$; $A_\Psi = 0.045$, ($v_{\Psi 0} = 5$, $v_{\Psi 1} = 9$).FIG. 3: v versus r along lines of constant u for two cases of weak pulses. All lines with $u \leq 24$ comes to the same r when $v \rightarrow \infty$.4(a): Case: $A_\Phi = 0$; $A_\Psi = 0.01$, ($v_{\Psi 0} = 5$, $v_{\Psi 1} = 9$).4(b): Case: $A_\Phi = 0$; $A_\Psi = 0.045$, ($v_{\Psi 0} = 5$, $v_{\Psi 1} = 9$).FIG. 4: Kretschmann curvature scalar along lines of constant u for two cases of weak pulses. All lines inside the BH ($u \leq 24$) is seen to increase when $v \rightarrow \infty$.

of r versus v along $u = \text{const}$ asymptotically tend to $r = r_{\text{Cauchy}}$ for u big enough.

The sharp increase of the mass-function for the greater v inside the BH (for $v \gtrsim 12$) in Fig. 2(a) is the result of the mass inflation which still works in the case of an exotic radiation pulse.

The Kretschmann scalar along $u = \text{const}$ is shown in Fig. 4(a). It is seen to increase with v for high values of $u = \text{const}$. The exponential increase of the Kretschmann scalar with v is a fingerprint of coming to the weak singularity at $v = \infty$. Thus in this case, probably the weak singularity exists at the Cauchy horizon.

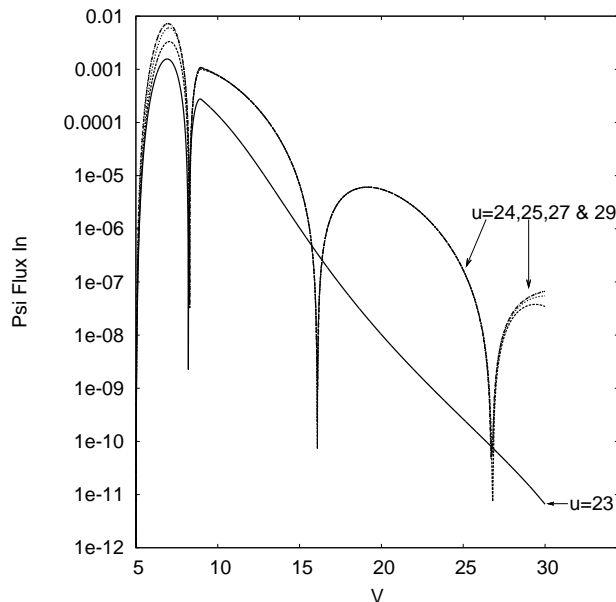
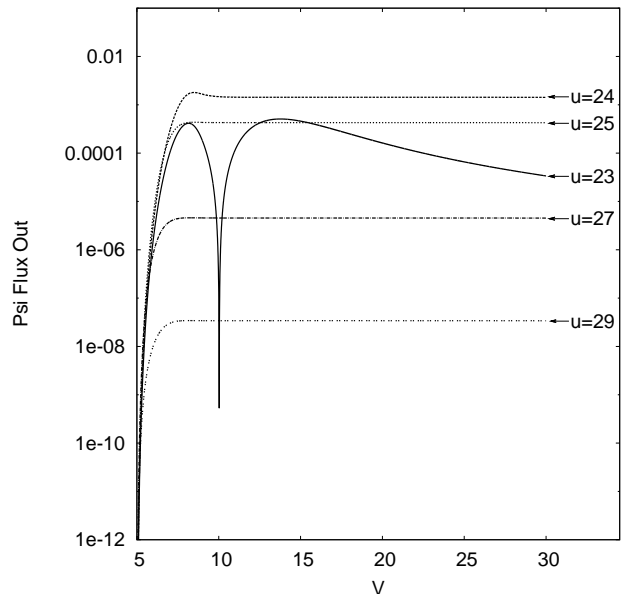
5(a): Ingoing flux T_{vv}^{Ψ} along lines of constant u .5(b): Outgoing flux T_{uu}^{Ψ} along lines of constant u .

FIG. 5: In- and outgoing Ψ fluxes of the negative energy for the case: $A_{\Phi} = 0$; $A_{\Psi} = 0.01$ ($v_{\Psi 0} = 5$, $v_{\Psi 1} = 9$). The initial ingoing pulse can be clearly seen (fig. 5a, between $5 \leq v \leq 9$), as can the scattered fluxes of the initial pulse.

Fig. 5(a) represents the evolution of the in-flux, T_{vv} , of the negative scalar energy into the BH. Fig. 5(b) shows the corresponding T_{uu} out-flux which arises as a result of the T_{vv} flux being scattered by the space-time curvature. The tails of the T_{vv} flux are the result of backscattering of the T_{uu} flux and so on and so forth.

In both Fig. 5(a) and Fig. 5(b) one can see the resonances arising as a result of the scattering process. These resonances are typical also for the cases of the irradiation by the more intense pulses.

Now let us consider the case of a more intense pulse of negative energy, but still not strong enough to destroy the BH. We consider the case

$$A_{\Phi} = 0; \quad A_{\Psi} = 0.045, \quad (v_{\Psi 0} = 5, \quad v_{\Psi 1} = 9) \quad (20)$$

First of all we note the following; In Fig. 2(b) one can see that at $u = 0$ the value of the mass function after the pulse $v > 9$ corresponds to the external mass $m \approx 0.945$. This is less than $q = 0.95$ which means, that if this value does not change when one comes to the OAH, the BH must be destroyed. But because of the scattering process, part of the negative energy of the pulse will be scattered away during the propagation of the pulse from $u = 0$ to the OAH and the amount of the negative energy pumped into the BH will be smaller. As a consequence, the final mass of the BH after the end of the whole process will be $m \approx 0.959$, and the position of the OAH process will be $u \approx 23.6$, see Fig. 6. Thus the BH survives.

The reason for the increase of the mass function (in Fig. 2(b)) in the region just after $v \approx 10$ for great u is mainly the additional flux of the negative energy T_{uu}

which arise because of the scattering effect (analogous to the scattering demonstrated in Fig. 5) and for bigger v it is a mild mass inflation.

The properties of the Kretschmann scalar inside of the BH is now more complicated. At big u it shows growing oscillations with v , see Fig. 4(b). These oscillations are the consequence of the oscillations of the T_{uu} and T_{vv} fluxes which are the analogues to those in Fig. 5.

Finally in Fig. 6 one can see the general structure of the R - and T -regions. For all situations we will call the OAH the horizon which is practically the border of the BH. The IA_{H1} is the border between the T_- -region and the internal R -region and its continuation. The horizon IA_{H2} is the border between the internal R and T_+ regions and its continuation. All these horizons can be seen in Fig. 6. Most interesting is the fact that the border IA_{H2} is not along a null-geodesic line (Cauchy Horizon) but comes to be visible inside the domain of integration.

On the basis of our computations and their analysis we may guess at the Penrose diagram in Fig. 7 for the case when the BH survives after being irradiated by a pulse of the exotic scalar field.

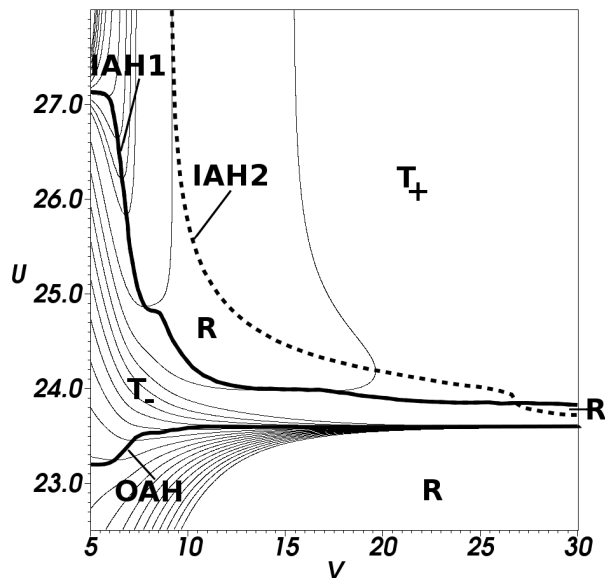


FIG. 6: Lines of constant r (thin lines, decreasing from bottom to top), positions of R - and T -regions and positions of the apparent horizons (thick lines) for the case of $A_\Phi = 0$; $A_\Psi = 0.045$, ($v_{\Psi_0} = 5$, $v_{\Psi_1} = 9$). In this case, the BH survives as can be seen by the OAH and IA1 not meeting.

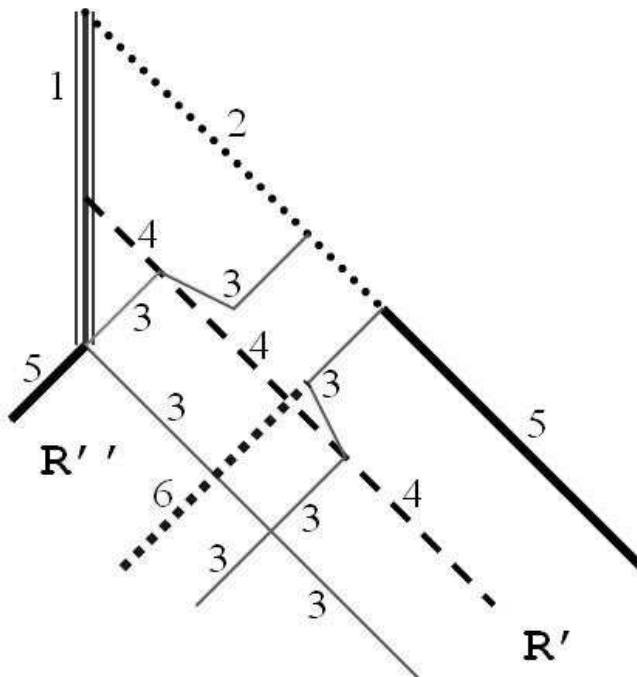


FIG. 7: The Penrose diagram for the case when the BH survives after being irradiated by a pulse of the exotic scalar field. Here: 1 – strong, $r = 0$, timelike singularity, 2 – weak singularity, 3 – horizons, 4 – narrow pulse of the exotic scalar field, 5 – light infinity, R' – our universe, R'' – another universe, 6 – the event horizon.

B. Destruction of the BH

Next we consider the following cases with (higher) negative energies of the exotic pulse:

$$A. \quad A_\Phi = 0; \quad A_\Psi = 0.05045 \quad (21)$$

$$B. \quad A_\Phi = 0; \quad A_\Psi = 0.0513 \quad (22)$$

$$C. \quad A_\Phi = 0; \quad A_\Psi = 0.0700 \quad (23)$$

In all cases $v_{\Psi_0} = 5$, $v_{\Psi_1} = 9$. Figs. 8(a)- 8(c) show the further evolutions of the general picture of the R and T regions for these cases.

In all these cases, the total power of the exotic pulse is large enough to reduce the mass of the object in the critical region $u \approx [23.2; 23.9]$ (where the OAH formed for the previous cases), to below the critical value $m_{crit} = q = 0.95$, see Fig. 9. Thus even after the reduction of the power of the pulse during the propagation from $u = 0$ to $u \approx 23.2$ due to the scattering, it is strong enough to destroy the BH.

This means that the outer and inner apparent horizons should meet and disappear. This process is seen in Fig. 8(a) and even more clearly in Fig. 8(b), which shows the slightly stronger case (22).

For these cases, for high v , the BH is converted into an object where the outer R and inner R -regions are connected. Now the test photons $u = const$ for all value of u go to bigger r , when $v \rightarrow \infty$.

For all cases (21-23) the mass-function does not demonstrate a mass inflation effect, see Fig. 9. We note that for the cases (21) and (22) the mass function for big v and big u does becomes greater than $m = 0.95$. However, this is related to the scattering of the exotic scalar field outside to bigger r . Of cause this is possible in the case of dynamical BHs. In this region (big v and big u) we are at big r , definitely outside the (dynamical) BH which is at smaller v .

For the cases (21-22) the Kretschmann scalar does not increase with v , but rather oscillates (see Figs. 10). These oscillations are the consequences of the oscillations of the T_{vv} -in flux (and also T_{uu} -out flux), which we described for the pulses with the smaller power, see Fig. 5(a)- 5(b).

The fact that the Kretschmann scalar does not increase exponentially with v , together with the fact that the mass function does not increase exponentially, indicates the absence of space-time singularities (excluding the timelike $r = 0$ singularity of the Reissner-Nordström BH beyond the top-left corner of the computational domain).

Finally, in Fig. 8(c) is shown the horizon structure for the case (23).

In this case, the exotic pulse is so powerful that the inner and outer apparent horizons meet quite fast and after this, there are not any horizons or borders left at all (to the right of $v \sim 7.5$). The outgoing signal $u = const$ can freely propagate away through the R -region. Also, the mass function becomes essentially smaller then q (see Fig. 9(c)), while the Kretschmann scalar becomes smaller and smaller with bigger v (see Fig. 10(c)). There

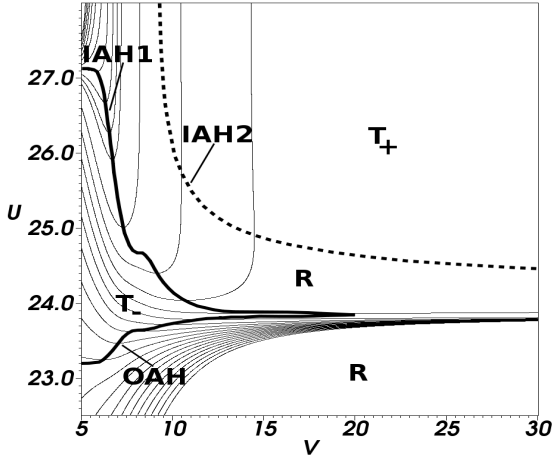
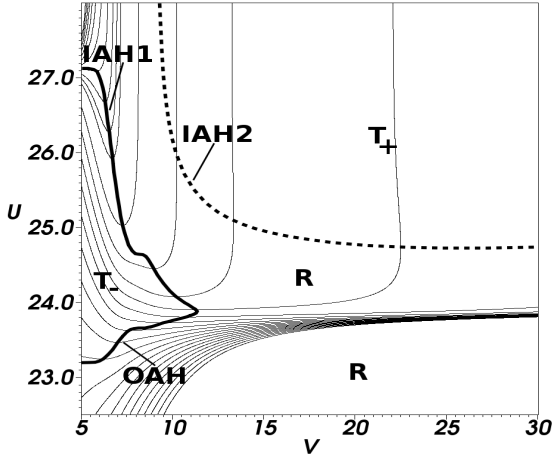
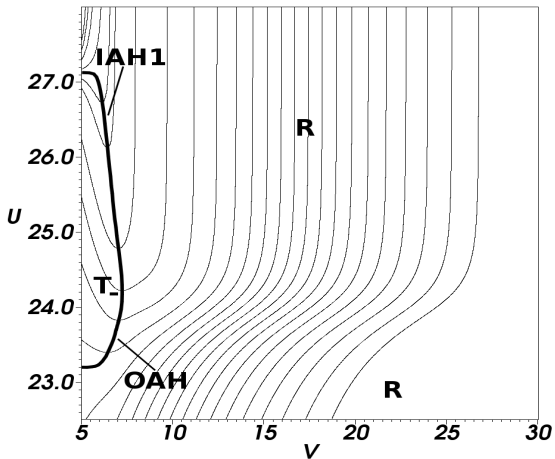
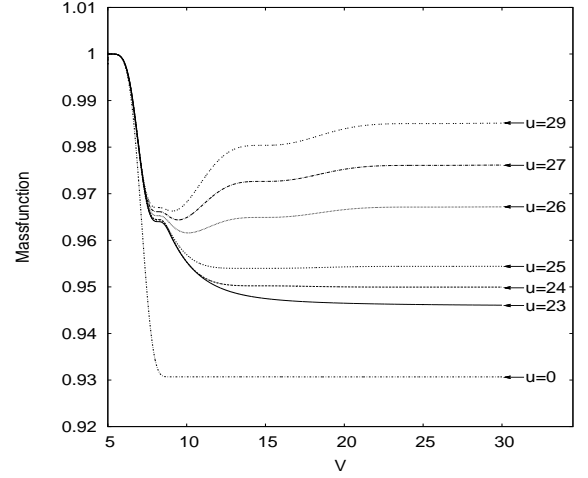
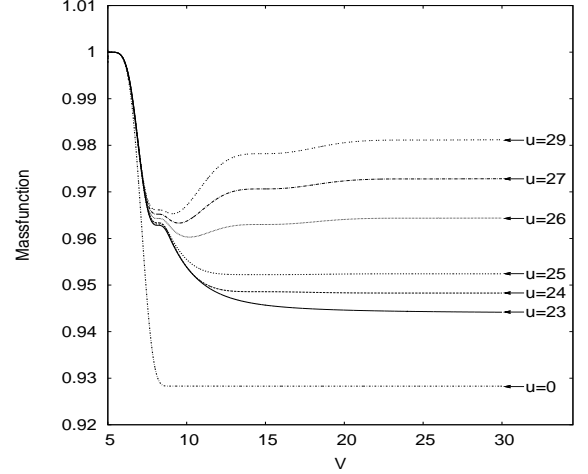
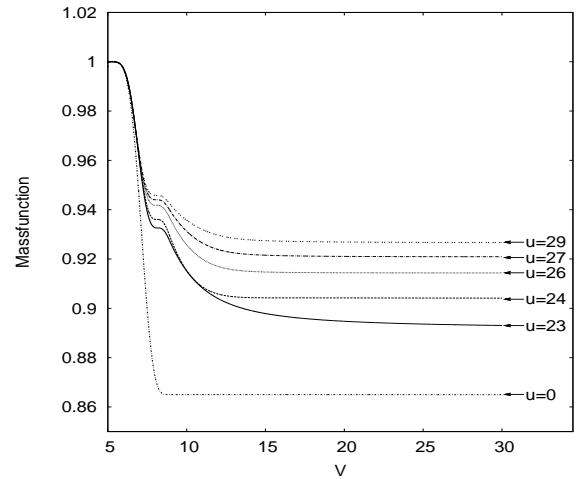
8(a): Case: $A_\Phi = 0$; $A_\Psi = 0.05045$.8(b): Case: $A_\Phi = 0$; $A_\Psi = 0.0513$.8(c): Case: $A_\Phi = 0$; $A_\Psi = 0.070$.9(a): $A_\Psi = 0.05045$ 9(b): $A_\Psi = 0.0513$ 9(c): $A_\Psi = 0.070$

FIG. 8: Lines of constant r (thin lines, decreasing from bottom to top), positions of R - and T -regions and positions of the apparent horizons (thick lines) for the cases a) $A_\Psi = 0.05045$; b) $A_\Psi = 0.0513$; c) $A_\Psi = 0.070$. In all cases ($v_{\Psi_0} = 5$, $v_{\Psi_1} = 9$) and in all cases the BH is destroyed as can be clearly seen by the meeting of the horizons.

FIG. 9: The mass function along lines of constant u for the cases: a) $A_\Psi = 0.05045$; b) $A_\Psi = 0.0513$; c) $A_\Psi = 0.070$. In all cases $A_\Phi = 0$; ($v_{\Psi_0} = 5$, $v_{\Psi_1} = 9$) and in all cases the BH is destroyed.

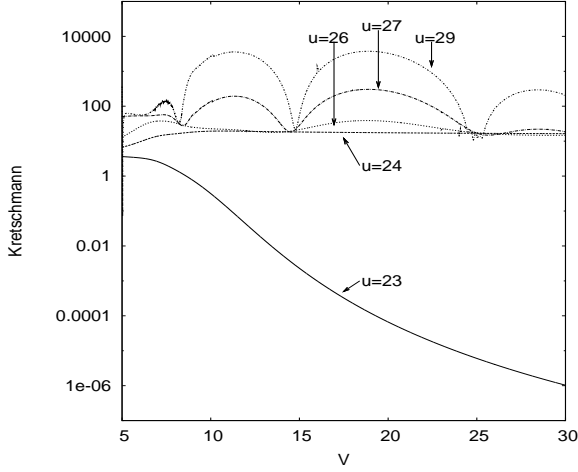
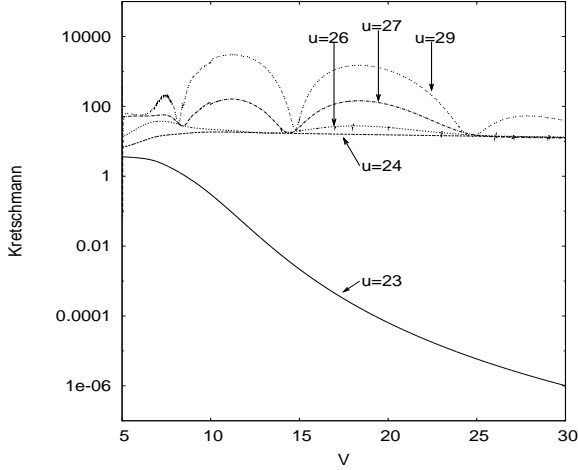
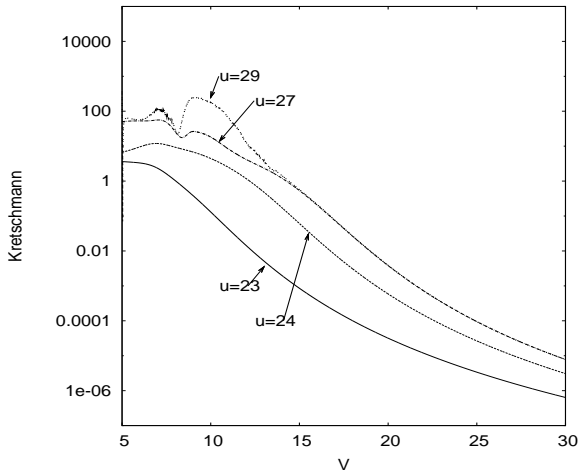
10(a): Case: $A_\Psi = 0.05045$ 10(b): Case: $A_\Psi = 0.0513$ 10(c): Case: $A_\Psi = 0.070$

FIG. 10: Kretschmann scalar along lines of constant u for the cases: a) $A_\Psi = 0.05045$; b) $A_\Psi = 0.0513$; c) $A_\Psi = 0.070$. In all cases $A_\Phi = 0$, ($v_{\Psi 0} = 5$, $v_{\Psi 1} = 9$) and in all cases the BH is destroyed.

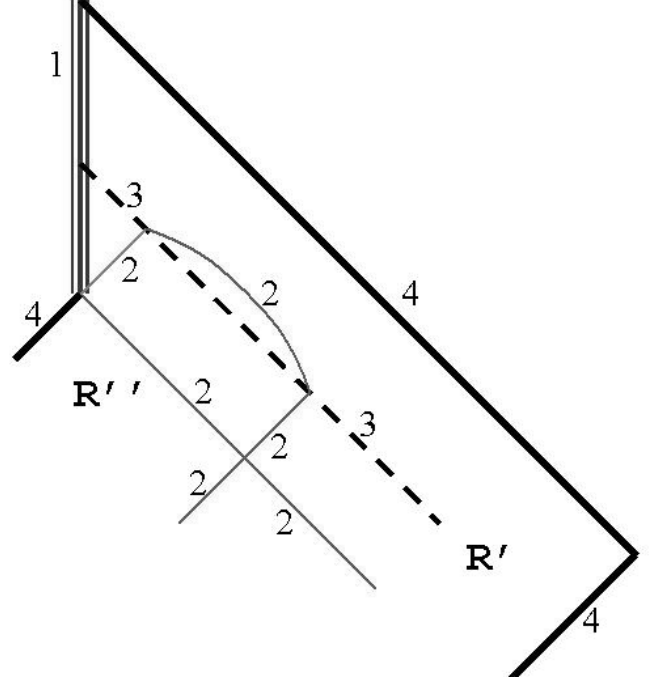


FIG. 11: The Penrose diagram for the case when the BH is destroyed after being irradiated by a pulse of the exotic scalar field. Here: 1 – strong singularity $r = 0$, 2 – horizons, 3 – narrow pulse of the exotic scalar field, 4 – light infinity, R' – our universe, R'' – another universe.

are not any singularities present (except for the timelike $r = 0$ singularity).

Fig. 11 represents the Penrose diagram that is confirmed by our numerical simulations for the cases when the BH is destroyed by the radiation.

At the end of this section we note the following. When the Reissner-Nordström BH is irradiated by a pulse of the exotic scalar radiation, the OAH becomes smaller (or disappears completely) and part of the outgoing radiation from the T_- region can go to the outer R' -region in our Universe. This radiation may come into the T_- region from the R'' -region that belongs to another Universe, which is the counterpart of the outer R' -region of Fig. 11 in our Universe (from the left hand side of Fig. 11 outside the computational domain). This means that it is possible for some radiation from the other Universe to come to our R' -region. The propagation of the radiation in the opposite direction, from our R' -region to the R'' -region in the other Universe, is still impossible. We call such an object a semitraversable wormhole [50].

IX. THE CASE OF THE IRRADIATION BY BOTH NORMAL AND EXOTIC PULSES

Finally we consider the case:

$$\begin{aligned} A_\Phi &= 0.4, & (v_{\Phi 0} = 5, & v_{\Phi 1} = 7) \\ A_\Psi &= 0.2, & (v_{\Psi 0} = 10, & v_{\Psi 1} = 12). \end{aligned} \quad (24)$$

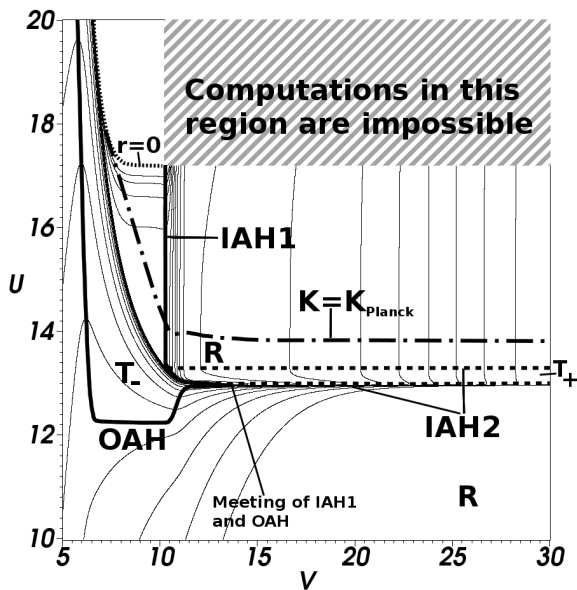


FIG. 12: Lines of constant r (thin lines, decreasing from bottom to top), positions of $r = 0$, $K = K_{\text{Planck}}$, apparent horizons and R - and T -regions for case: $A_\Phi = 0.4$, ($v_{\Phi 0} = 5$, $v_{\Phi 1} = 7$); $A_\Psi = 0.2$, ($v_{\Psi 0} = 10$, $v_{\Psi 1} = 12$) in which the BH is destroyed.

In this case, the Reissner-Nordström BH is irradiated at the beginning by a strong pulse of the normal scalar field which causes a strong spacelike $r = 0$ singularity to arise in the T_- -region inside the BH (similar to the cases investigated in [33]). After that, at higher v , the BH is then irradiated by a strong pulse of the exotic scalar field.

For this case, one can see strong nonlinear processes. Fig. 12 shows the general structure of the apparent horizons and the position of the (spacelike) singularity $r = 0$. There is also a line showing the position of the Kretschmann scalar equal to its Planckian value of $K = (G\hbar/c^3)^{-2} \approx 10^{131} \text{cm}^{-4}$. Beyond this border the classical General Relativity is not applicable and we consider this region as a singularity from the classical point of view. Our calculations are thus not reliable for this region and we will not consider it (upper-right part of Fig. 12, above the line $K = K_{\text{Planck}}$). We would like to do the following remark about the K -scalar. This scalar has dimension cm^{-4} in the CGS -units system. In the paper [33] and in this paper we represent all figures in dimensionless units. For the figures, we draw the K -scalar (and the value of the Planckian K -scalar) for the case when the linear scale (the size of the BH in this paper) is equal to unity.

The Kretschmann scalar is represented in Fig. 13. For large $u \geq 14$, the Kretschmann scalar grows catastrophically fast and reach the singularity $K = K_{\text{Planck}}$. This is the consequence of the influence of the first pulse, with the positive energy density. This is the same process which we analyzed in [33], see e.g. Fig. 13 in [33]. Along

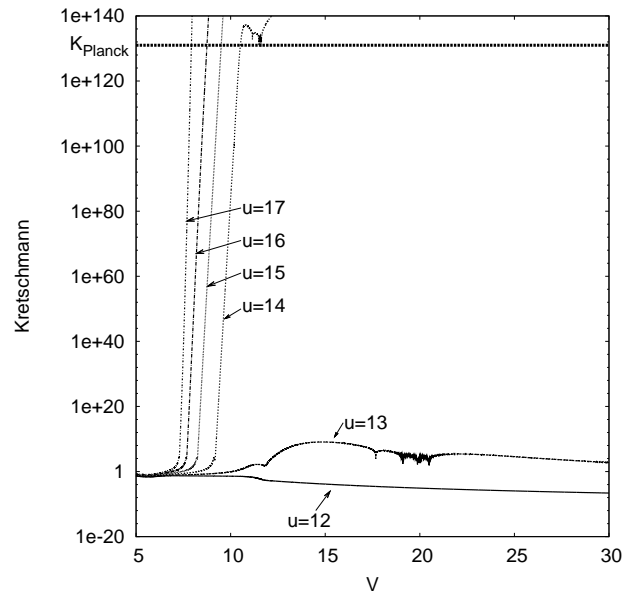


FIG. 13: Kretschmann scalar versus v along lines of constant u for case: $A_\Phi = 0.4$, ($v_{\Phi 0} = 5$, $v_{\Phi 1} = 7$); $A_\Psi = 0.2$ ($v_{\Psi 0} = 10$, $v_{\Psi 1} = 12$). Also, the location of the Kretschmann singularity K_{Planck} is plotted.

$u = 12$, the Kretschmann scalar decreases with increasing v , this is of course as expected as this line is always outside of any horizon (fig. 12). The behavior along the line $u = 13$ is somewhat in between, for small v ($v \lesssim 14$), the Kretschmann scalar shows a slight tendency to increase. However, for larger v , the BH is destroyed and the Kretschmann scalar shows a decreasing behaviour. Also cf. with the discussion of the mass function below.

In Fig. 14 (showing r versus v), the test photons along $u = 18$ reaches $r = 0$. Photons in the range $13 \lesssim u \lesssim 17$ come close to $r = 0$ and after that, they propagate to larger r (after the meeting with the pulse of the exotic scalar field at $10 \lesssim v \lesssim 12$). However, it is reminded that photons along $u \gtrsim 14$ meet with $K = K_{\text{Planck}}$ and thus effectively reach the singularity before they can escape to higher r . The photons along $u = 12$ constantly go to bigger r because they are always outside of any horizon.

In Fig. 15, it is seen that the mass function goes up for all lines of $u = \text{constant}$ between $5 \leq v \leq 7$, this is merely the trivial effect of mass being pumped into the BH by the positive energy pulse. In addition to this, the mass function for $u \geq 14$ continues to increase even after the passage of the positive energy pulse, due to the processes described in section VII until they reach the $K = K_{\text{Planck}}$ singularity.

As the negative energy pulse goes into the BH, the mass function along lines $u \leq 13$ decreases due to the negative energy contents of the second pulse. This second pulse, causes the mass function to become less than q in the region near the outer horizon and it leads to the meeting of the inner and outer apparent horizons and the

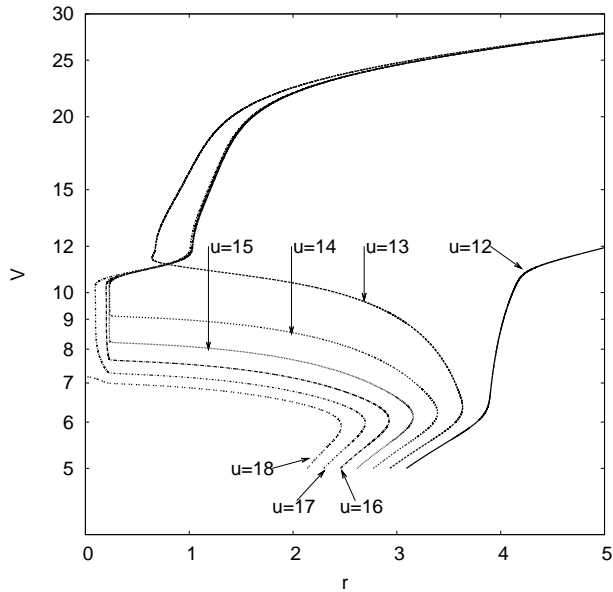


FIG. 14: r versus v along constant lines of constant u for case: $A_\Phi = 0.4$, ($v_{\Phi 0} = 5$, $v_{\Phi 1} = 7$); $A_\Psi = 0.2$, ($v_{\Psi 0} = 10$, $v_{\Psi 1} = 12$). All lines for $u \geq 17$ can in principle escape to infinity, except that most of them hit the Kretschmann singularity (see text for details).

disappearance of the BH around $v \approx 14$ (see figure 12). Along $u = 12$, the mass function continues to decrease because of the scattering processes of the exotic scalar field. Along $u = 13$, however, we see that the mass function increases drastically near $v \approx 12$. This growth is probably caused by the mass inflation effect, since in this region we are close to the border of the BH, but still inside it. The apparent horizons do not meet and the BH is not destroyed until around $v \approx 14$. In the same region, one can also see a modest growth of the Kretschmann scalar in Fig. 13. However, as the BH is destroyed around $v \approx 14$, we see that the mass function halts its growth and the Kretschmann scalar starts to decrease.

X. CONCLUSIONS

The processes arising when a Reissner-Nordström BH is irradiated by a pulse of an exotic scalar field with a negative energy density have been analyzed. We have performed the corresponding numerical computations using a numerical code specially designed for the purpose. It was demonstrated that these processes are quite different from the processes arising in the case of the irradiation of a Reissner-Nordström BH by a pulse of a normal scalar field.

The evolution of the mass function and the Kretschmann scalar demonstrate that in the case of the exotic scalar field, the evolution does not lead to the origin of a strong spacelike singularity $r = 0$ in the T -region

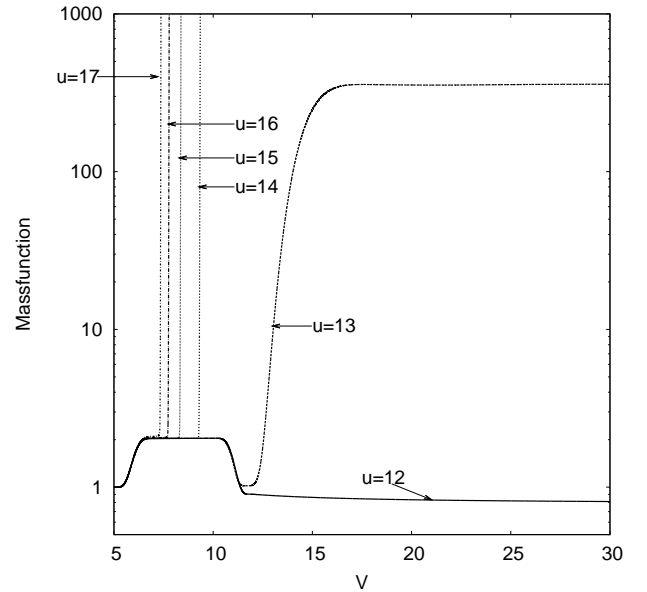


FIG. 15: Mass function along lines of constant u for case: $A_\Phi = 0.4$, ($v_{\Phi 0} = 5$, $v_{\Phi 1} = 7$); $A_\Psi = 0.2$, ($v_{\Psi 0} = 10$, $v_{\Psi 1} = 12$). Effects of both the normal and the exotic scalar pulse are clearly seen.

as was the seen in the case of irradiation by the normal scalar field [33].

The numerical calculations demonstrate the manifestation of the antifocusing effects in the gravity field of an exotic scalar field with a negative energy density.

When the power of the exotic pulse with negative energy density is great enough, the mass function becomes less than the charge q near the outer apparent horizon. As a result the BH disappears. This process was analyzed in detail.

Acknowledgements

We thank the unknown referees of our paper for very constructive criticism and helpful advice. This work was supported in part by the JSPS Postdoctoral Fellowship For Foreign Researchers, the Grant-in-Aid for Scientific Research Fund of the JSPS (19 – 07795), Russian Foundation for Basic Research (project codes: 07 – 02 – 01128 – *a*, 08 – 02 – 00090 – *a*, 08 – 02 – 00159 – *a*), scientific schools: *NSh* – 626.2008.2, *Sh* – 2469.2008.2 and by the program *Origin and Evolution of Stars and Galaxies 2009* of the Russian Academy of Sciences.

Appendix A: Convergence of the code

In this appendix, we demonstrate that our numerical code is converging (to a physical solution) when including the effects of nontrivial Φ and Ψ fields. The results

presented here are very similar to those presented in [34] as could be expected, since the codes in that paper and this are essentially identical. For this reason, for further details of the code, we refer to [34].

The initial conditions for the tests in this Appendix are similar to those described in section IX, i.e. the initial conditions are those of a Reissner-Nordstrom BH, perturbed by first an in-falling Φ field (from $v = [5; 7]$ with amplitude: $A_\Phi = 0.4$) and subsequently by an in-falling Ψ field (from $v = [10; 12]$ with amplitude: $A_\Psi = 0.2$). Our computational domain for the convergence tests are, as for all simulations in this paper, in the range $v = [5; 30]$ and $u = [0; 30]$. This setup is the most complicated one that we have done in this paper (in that it incorporates the dynamic effects of both Φ and Ψ fields) and leaves no trivial terms left in the evolution equations, thus it is a good test for the convergence of our code.

Here we demonstrate the convergence of the code by comparing a series of simulations with varying numerical resolution. For the tests in this Appendix, we do a total of 6 simulations, with each simulation changing the AMR base resolution and refinement criteria in such a way as to mimic doubling the numerical resolution from one simulation to the next (for further details and more thorough discussions, see [34, 44]).

To limit the number of plots in this Appendix, we concentrate on displaying convergence results along the line $u = 17$ (however, it should be noted that a large number of convergence tests has been carried out and that the results presented in this Appendix are representative of the convergence properties of the code in other parts of the computational domain and for other configurations of the initial data). As can be seen in figure 12, this line is very close to the $r = 0$ singularity (where we can expect strong dynamics) as well as inside the Kretschmann singularity and thus convergence along this line is a good indication of the convergence behavior throughout the computational domain.

Along this line, we calculate the relative convergence between two simulations (one with a numerical resolution twice that of the other) relative to a simulation with very high resolution:

$$\xi(x_N^i) \equiv \frac{|x_N^i - x_{2N}^i|}{|x_{HighRes}^i|} \quad (\text{A1})$$

where x_N^i denotes the dynamic variable x at the i -th grid point of simulation with resolution N and where $x_{HighRes}^i$ denotes the dynamic variable of the same i 'th point for a simulation with the highest numerical resolution done by us. Obviously, this expression only makes sense for those i points that coincide in all simulations.

Figures 16(a)- 16(d) show the relative convergence, ξ , for the dynamic variables r, σ, Φ and Ψ respectively. The lines in the figures are marked by their numerical resolution measured in terms of the most coarse resolution N_0 , the high resolution simulation used to calculate expression (A1), has a numerical resolution of 32 times the

base resolution, i.e. $N = 32N_0$.

From these figures, it is clearly seen that the four dynamic variables are converging for simulations of increasing resolution. Furthermore, since we plot the *relative* convergence of the dynamic variables, we see that the relative change between the two highest resolution simulations show that the variables change 0.1% or less, which must be considered a quite acceptable convergence. We note that a closer analysis of the data in figures 16(a)- 16(d) has revealed that the dynamic variables are indeed converging with second order accuracy as was expected based on analyses and tests performed in [33, 34].

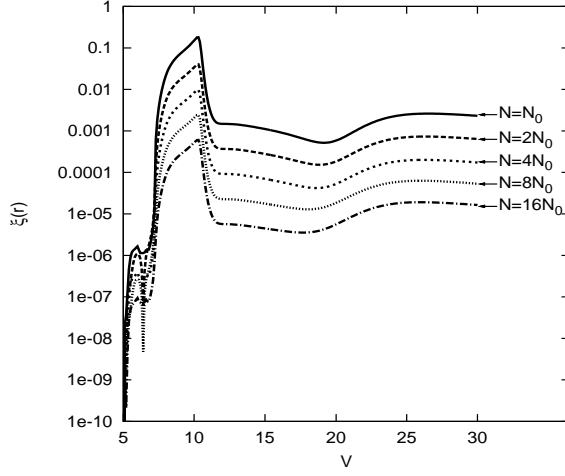
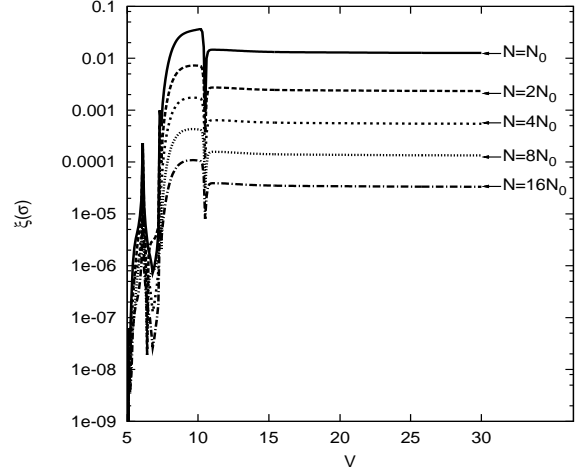
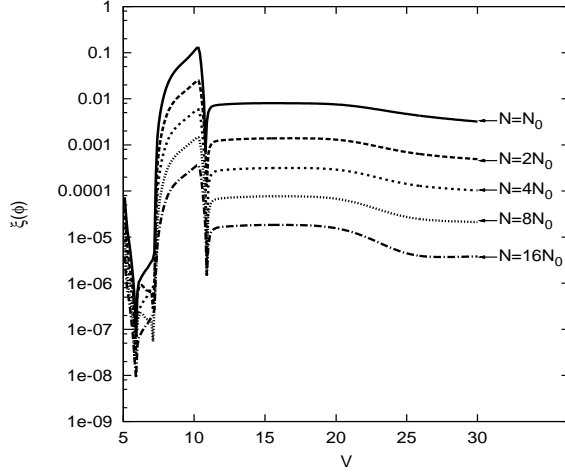
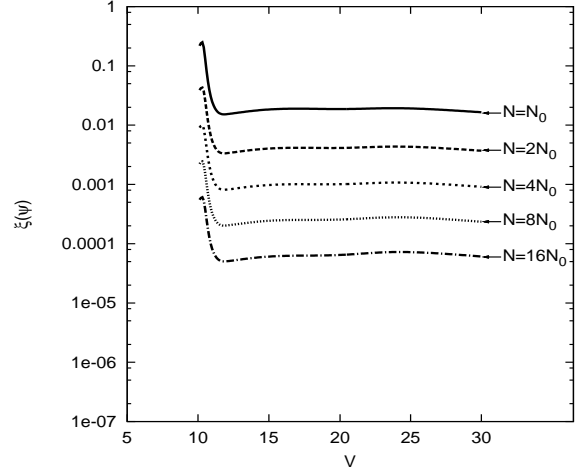
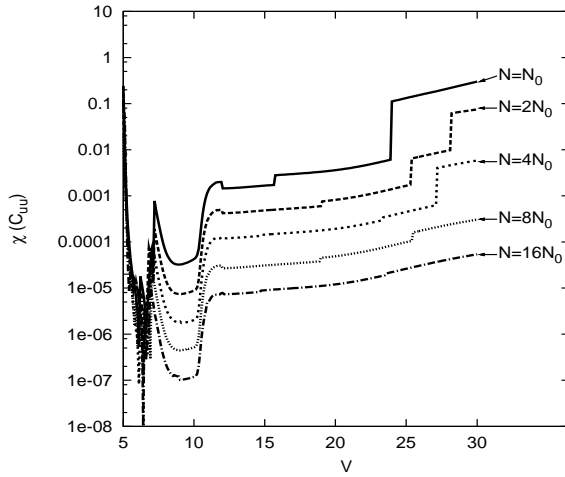
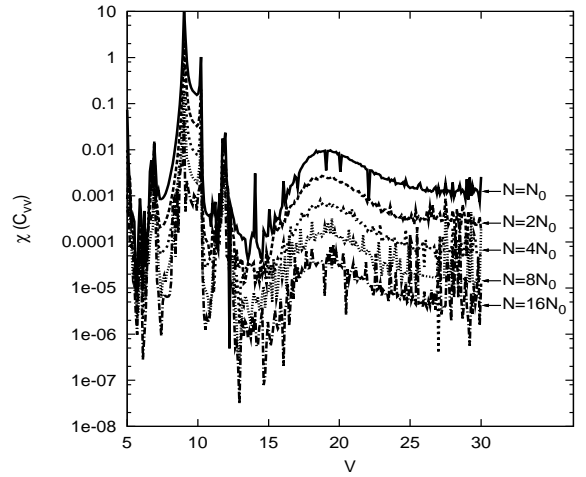
However, of course it is not enough to demonstrate that the simulations are converging, they must also converge to a physical solution, i.e. the residuals of the constraint equations (eqs. (6) and (7)) must converge to zero. To demonstrate this, we calculate the relative convergence of the constraint equation residuals, (relative to the Einstein-tensor, eqs. (2a) and (2b) respectively) in a similar way to eq. (A1) :

$$\chi(C_N^i) \equiv \frac{|C_N^i|}{|G_{HighRes}^i|} \quad (\text{A2})$$

where C_N^i denotes the residual of the constraint equation, (C_{uu} or C_{vv}), at the i 'th point for simulation with resolution N and where $G_{HighRes}^i$ denotes the corresponding Einstein-tensor component (G_{uu} or G_{vv} respectively) at the same point.

The relative convergence of the residuals of the constraint equations are demonstrated in figures 16(e) and 16(f) where it is seen that they converge towards zero for higher resolution simulations. This indicates that not only are the numerical solutions converging for simulations of higher resolution, but that they are indeed converging towards a physical solution. The convergence plots for the constraint equations exhibit significant more numerical noise than the convergence plots for the basic dynamic variables. However, it is reminded that the constraint equations are derived quantities of the basic dynamic variables, therefore the constraint equations will be less accurate and include more numerical errors such as truncation errors from calculating the derivatives of the basic dynamic variables and errors associated with calculating derivatives in the AMR mesh. Nevertheless, figs. 16(e) and 16(f) indicate that the solutions are indeed converging to the physical solutions for high resolutions.

Finally it should be noted that the convergence results presented in this appendix are not the only convergence tests that we have performed, they merely represent typical results of the convergence behavior of the code. For all results presented in this paper, we have performed a large number of simulations with varying resolutions to ensure that the results had converged to their physical solution.

16(a):Relative convergence of r .16(b):Relative convergence of σ .16(c):Relative convergence of Φ .16(d):Relative convergence of Ψ .16(e):Relative convergence of C_{uu} .16(f):Relative convergence of C_{vv} .FIG. 16: Relative convergence of the dynamic variables and constraint equations along line of $u = 17$, see text for details.

-
- [1] R. Penrose, *Structure of Space-Time* (Battelle Recontres, 1968), eds. C. M. De Witt, J. A. Wheeler and N. Y. Benjamin.
- [2] A. Doroshkevich and I. D. Novikov, *Zh. Eksp. Teor. Fiz.* **74**, 3 (1978).
- [3] J. M. M. Namara, *Proc. Roy. Soc. Ser A* **358**, 499 (1978).
- [4] J. M. M. Namara, *Proc. Roy. Soc. Ser A* **364**, 121 (1978).
- [5] Y. Gursel, V. D. Sandberg, I. D. Novikov, and A. A. Starobinsky, *Phys. Rev. D* **19**, 413 (1979).
- [6] Y. Gursel, I. D. Novikov, V. D. Sandberg, and A. A. Starobinsky, *Phys. Rev. D* **20**, 1260 (1979).
- [7] R. A. Matzner, N. Zamorano, and V. D. Sandberg, *Phys. Rev. D* **19**, 2821 (1979).
- [8] S. Chandrasekhar and J. B. Hartle, *Proc. Roy. Soc. Ser. A* **384**, 301 (1982).
- [9] D. S. Goldwirth and T. Piran, *Phys. Rev. D* **36**, 3575 (1987).
- [10] E. Poisson and W. Israel, *Phys. Rev. D* **41**, 1796 (1990).
- [11] A. Ori, *Phys. Rev. Lett.* **67**, 789 (1991).
- [12] A. Ori, *Phys. Rev. Lett.* **68**, 2117 (1992).
- [13] M. Gnedin and N. Gnedin, *Class. Quant. Grav.* **10**, 1083 (1993).
- [14] A. Bonanno, S. Droz, W. Israel, and S. Morsink, *Proc. Roy. Soc. London A* **450**, 553 (1995).
- [15] P. R. Brady and J. D. Smith, *Phys. Rev. Lett.* **75**, 1256 (1995).
- [16] S. Droz, *Helv. Phys. Acta* **69**, 257 (1996).
- [17] L. M. Burko and A. Ori, *Internal structure of black holes and spacetime singularities* (Jerusalem, ISBN 0-7503-05487, 1997), 13 of the *Annals of the Israel Physical Society*.
- [18] L. M. Burko, *Phys. Rev. Lett.* **79**, 4958 (1997).
- [19] S. Hod and T. Piran, *Phys. Rev. D.* **55**, 3485 (1997).
- [20] L. M. Burko and A. Ori, *Phys. Rev. D.* **57**, R7084 (1998).
- [21] S. Hod and T. Piran, *Gen. Rel. Grav.* **30**, 1555 (1998).
- [22] S. Hod and T. Piran, *Phys. Rev. Lett.* **81**, 1554 (1998).
- [23] L. M. Burko, *Phys. Rev. D.* **59**, 024011 (1998).
- [24] L. M. Burko, *Phys. Rev. D.* **60**, 104033 (1999).
- [25] A. Ori, *Phys. Rev. Lett.* **83**, 5423 (1999).
- [26] A. Ori, *Phys. Rev. D* **61**, 024001 (1999).
- [27] L. M. Burko, *Phys. Rev. D.* **66**, 024046 (2002).
- [28] B. K. Berger, *Living Reviews in Relativity* **5** (2002), URL <http://www.livingreviews.org/lrr-2002-1>.
- [29] L. M. Burko, *Phys. Rev. Lett.* **90**, 121101 (2003), erratum in *Phys. Rev. Lett.* **90**, 249902(E).
- [30] Y. Oren and T. Piran, *Phys. Rev. D.* **68**, 044013 (2003).
- [31] A. J. S. Hamilton and S. E. Pollack, *Phys. Rev. D* **71**, 084031 (2005).
- [32] A. J. S. Hamilton and S. E. Pollack, *Phys. Rev. D* **71**, 084032 (2005).
- [33] J. Hansen, A. Khokhlov, and I. Novikov, *Phys. Rev. D* **71**, 064013 (2005).
- [34] A. Doroshkevich, J. Hansen, I. Novikov, and A. Shatskiy, *I.J.Mod.Phys.D* **18**, 1665 (2009).
- [35] S. Krasnikov, *Phys. Rev. D* **62**, 084028 (2000).
- [36] S. V. Sushkov, *Phys. Rev. D* **71**, 043520 (2005).
- [37] E. Babichev, V. Dokuchaev, and Y. Eroshenko, *Phys.Rev.Lett.* **93**, 021102 (2004).
- [38] K. A. Bronnikov, *Acta Physica Polonica* **B 4**, 251 (1973).
- [39] K. A. Bronnikov and S. V. Sushkov (2010), ArXiv: gr-qc/1001.3511.
- [40] S. E. Hong, D. il Hwang, E. D. Stewart, and D. han Yeom (2008), arXiv: 0808.1709.
- [41] D. han Yeom and H. Zoe (2008), arXiv: 0811.1637.
- [42] J. A. González and F. S. Guzmán, *Phys. Rev. D* **79**, 121501 (2009).
- [43] L. M. Burko and A. Ori, *Phys. Rev. D* **56**, 7820 (1997).
- [44] F. Pretorius and L. Lehner, *J. Comput. Phys.* **198**, 10 (2004).
- [45] N. V. Gnedin and M. L. Gnedin, *Sov. Astron.* **36**, 296 (1992).
- [46] I. D. Novikov, *General Relativity and Gravitation* **33**, 2259 (2001).
- [47] I. D. Novikov, *Texas in Tuscany. XXI Symposium on Relativistic Astrophysics, Florence* pp. 77–90 (2003).
- [48] V. P. Frolov and I. D. Novikov, *Black Hole Physics* (Kluwer Academic Publishers, 1998).
- [49] E. I. Novikova and I. D. Novikov, *Phys. Rev. D* **81**, 104034 (2010).
- [50] D. Novikov, A. Doroshkevich, I. Novikov, and A. Shatskiy, *Astronomy Reports* **53**, 10791085 (2009).